Sensitivity of Nickel-Doped Zinc Ferrite Nanostructures Prepared by Reactive Sputtering

Vital Kumar Manoo, Ashok Singh Mehta, Ramaswami Mukherjee

Department of Physics, Savitribai Phule Pune University, Pune, INDIA

Abstract

This study examined the impact of substituting nickel for iron(III) in the normal spinel $ZnFe_2O_4$ crystal structure at electrochemical interfaces, either partially or completely. The resulting $ZnNi_xFe_{2-x}O_4$ nanostructures had a spherical morphology with an average particle size ranging from 15 to 45 nm. Their energy band gaps varied between 2.05 and 3.02 eV. All synthesized materials retained a normal spinel structure, attributed to the octahedral site preference energy (OSPE) of Zn^{2+}, Fe^{3+}, Co^{2+} and Ni^{2+} ions.

Keywords: Zinc ferrite; Nickel ferrite; Nanostructures; Reactive sputtering
Received: 09 January 2025; **Revised:** 01 March 2025; **Accepted:** 15 March 2025; **Published:** 1 April 2025

1. Introduction

Spintronics, or spin electronics, is a field of technology that exploits the intrinsic spin of electrons, along with their charge, to store and process information [1]. Unlike conventional electronics, which rely solely on charge transport, spintronics leverages spin polarization to enhance device performance, enabling faster processing, lower power consumption, and non-volatile memory storage. Key materials include magnetic semiconductors and ferromagnetic metals, with applications in magnetic random-access memory (MRAM), quantum computing, and advanced sensors [2-4]. Spintronic devices, such as spin valves and tunneling magnetoresistance (TMR) structures, are crucial in hard drives, logic circuits, and next-generation computing technologies [5,6].

Zinc ferrite ($ZnFe_2O_4$) is a versatile spinel-structured material with significant applications in electronics, catalysis, and energy storage [7]. It has a cubic crystal structure where Zn^{2+} ions occupy tetrahedral sites, while Fe^{3+} ions prefer octahedral coordination [8]. $ZnFe_2O_4$ exhibits semiconducting properties with a band gap ranging from 1.9 to 2.2 eV, making it useful in photocatalysis [9]. It has good thermal stability, moderate electrical conductivity, and ferrimagnetic behavior at low temperatures. $ZnFe_2O_4$ can be synthesized using various methods, including sol-gel, co-precipitation, hydrothermal, and solid-state reactions. These techniques influence particle size, morphology, and crystallinity [10-12]. Applications of $ZnFe_2O_4$ span multiple fields, such as gas sensors, lithium-ion batteries, water purification, and magnetic resonance imaging (MRI) [13-16]. It is also employed as a catalyst in environmental remediation and as an electrode material in supercapacitors. Its unique electrical and magnetic properties make it a promising material for future technological advancements [17,18].

Substituting ferromagnetic metallic ions like cobalt (Co^{2+}) and nickel (Ni^{2+}) in ferrite lattice structures significantly alters their magnetic, electrical, and optical properties [19-23]. This substitution modifies the distribution of cations between tetrahedral and octahedral sites, influencing parameters such as saturation magnetization, coercivity, and electrical resistivity. For instance, cobalt substitution enhances magnetic anisotropy, making it useful in high-density recording media, while nickel improves electrical conductivity for microwave and spintronic applications [24-26]. These modifications are crucial for optimizing ferrites in sensors, magnetic storage, catalysis, and biomedical applications, enabling tailored material properties for specific industrial and technological advancements [27-29].

In this work, the $ZnFe_2O_4$ nanostructures were synthesized and modified by substitution of Fe^{3+} ions in the ferrite lattice with nickel ions in two consecutive steps using reactive magnetron sputtering technique. The structural and morphological characteristics of the synthesized nanostructures were introduced and studied.

2. Experimental Work

Reactive magnetron sputtering is a widely used thin-film deposition technique for fabricating zinc ferrite ($ZnFe_2O_4$) and zinc-nickel ferrite ($ZnNi_xFe_{2-x}O_4$) nanostructures. The process involves the use of a magnetron sputtering system equipped with metallic or composite targets and an oxygen-containing plasma environment to facilitate oxide formation.

First, the deposition chamber was evacuated to

ultra-high vacuum (~10^{-6} Torr) to minimize contamination. Highly-pure Zn, Fe and Ni sheets were used as sputtering targets, and a controlled mixture of argon (Ar) and oxygen (O_2) was introduced to sustain the plasma and produce the oxide compound (ferrite). A DC power supply was applied to the target, generating a plasma that bombards the target material, ejecting atoms that react with oxygen to form ferrite thin films on the substrate. The substrate temperature, sputtering power, gas flow ratio, and deposition time were carefully optimized to achieve the desired stoichiometry and crystalline structure. The deposited films may undergo post-annealing at 500–800°C in an oxygen atmosphere to enhance phase purity, crystallinity, and magnetic properties. The final nanostructures are characterized using X-ray diffraction (XRD) and field-emission scanning electron microscopy (FE-SEM). This method allows precise control over composition and morphology, making it an efficient approach for fabricating high-performance $ZnFe_2O_4$ and $ZnNi_xFe_{2-x}O_4$ thin films for applications in spintronics, magnetic sensors, and catalysis.

3. Results and Discussion

When nickel is doped into $ZnFe_2O_4$ to form the $ZnNi_xFe_{2-x}O_4$ structure, significant changes in the crystalline structure are expected due to the differences in ionic radii and electronic configurations between Ni^{2+} and Fe^{3+} ions. $ZnFe_2O_4$ typically crystallizes in a normal spinel structure, where Zn^{2+} occupies tetrahedral sites and Fe^{3+} occupies octahedral sites. However, the introduction of Ni^{2+} ions, which have a strong preference for octahedral coordination, can lead to a partial or complete transition to an inverse spinel structure. In this case, Ni^{2+} ions may displace some Fe^{3+} ions from octahedral sites, causing structural rearrangement.

The lattice parameters of the spinel structure are also likely to change due to the smaller ionic radius of Ni^{2+} compared to Fe^{3+}. This substitution can lead to a contraction of the unit cell, resulting in a shift in XRD peaks toward higher angles. However, intermediate compositions ($0<x<2$) may exhibit peak shifts toward lower angles, indicating an expansion of the lattice due to the competing effects of Ni^{2+} incorporation and structural distortions. Additionally, the distribution of cations between tetrahedral and octahedral sites can influence magnetic and catalytic properties, as the arrangement of Ni^{2+} and Fe^{3+} ions affects superexchange interactions. These structural modifications make $ZnNi_xFe_{2-x}O_4$ a versatile material with tunable properties for applications in photocatalysis, magnetism, and photonics.

The XRD analysis was performed to examine the phase compositions and crystallite sizes of the samples. The XRD patterns of $ZnNi_xFe_{2-x}O_4$ (x = 0, 0.25, 0.5, 0.75, 1, 2) are presented in Fig. (1). For x=0 and x=2, the diffraction patterns align perfectly with those of the normal spinel structures $ZnFe_2O_4$ and $ZnNi_2O_4$. For intermediate compositions, ZnNixFe2-xO4 spinel remains the primary crystalline phase, but the patterns are shifted compared to both $ZnFe_2O_4$ and $ZnNi_2O_4$. Specifically, for x values between 0.25 and 1, the spinel peaks gradually shift toward lower angles as the Ni content increases. This shift suggests that materials with intermediate compositions may adopt a structure that is intermediate between $ZnFe_2O_4$ and $ZnNi_2O_4$ nanomaterials.

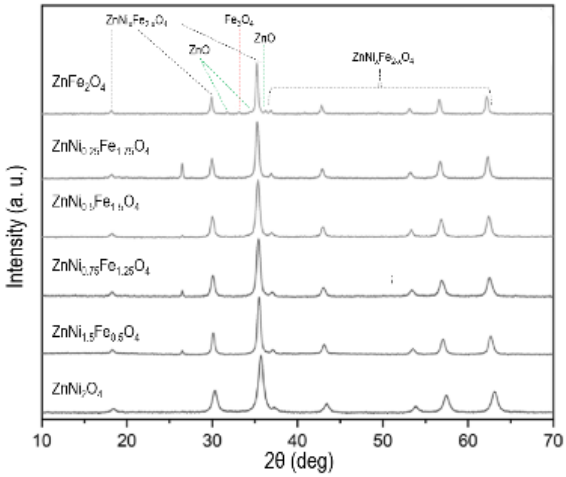

Fig. (1) XRD patterns of the $ZnNi_xFe_{2-x}O_4$ (x = 0, 0.25, 0.5, 0.75, 1, 2) nanostructure samples prepared in this work

The concentration of the test sample was varied while cyclic voltammograms were obtained at a constant scan rate of 80 mV/s as shown in Fig. (2). The oxidation current, averaged from three readings at each concentration, was used to create a calibration plot for each sensor. The sensitivity of each sensor, presented in table (1), is represented by the slope of the calibration plot. The $ZnFe_2O_4$ sensor exhibited the highest sensitivity (38 µA/mM), followed closely by the tailored $ZnNiFeO_4$ sensor.

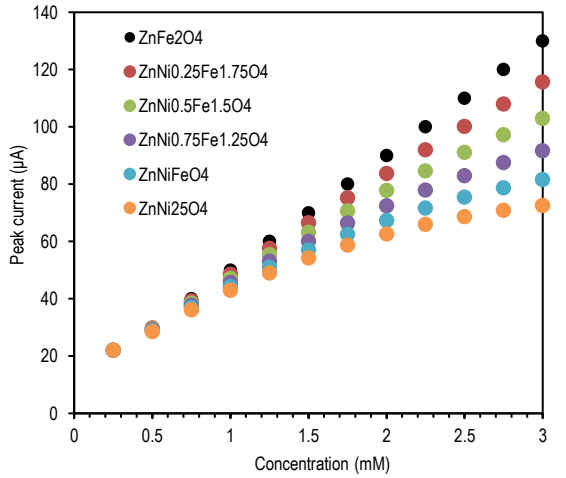

Fig. (2) Calibration of the $ZnNi_xFe_{2-x}O_4$ (x = 0, 0.25, 0.5, 0.75, 1, 2) sensors prepared in this work for the test sample concentration at pH = 77

The limit of detection (LOD) was calculated as LOD = KD/S, where K was set to 3 (statistical confidence level), D represents the standard deviation of blank measurements, and S is the sensor's sensitivity. The LOD values for each sensor are shown in table (1). The $ZnNiFeO_4$ sensor achieved the lowest LOD (1.8 µM), while the $ZnFe_2O_4$ sensor had the highest LOD (8.0 µM) among the sensors tested.

Table (1) Values of sensitivity and LOD for the $ZnNi_xFe_{2-x}O_4$ sensors fabricated in this work

Sample	Sensitivity (µA/mM)	LOD (µM)
$ZnFe_2O_4$	37.5-38.0	7.9-8.0
$ZnNi_{0.25}Fe_{1.75}O_4$	32.0-32.5	7.5-7.7
$ZnNi_{0.5}Fe_{1.5}O_4$	32.5-34.0	2.1-2.3
$ZnNi_{0.75}Fe_{1.25}O_4$	34.0-35.0	2.3-2.4
$ZnNiFeO_4$	35.5-36.0	1.8-1.9
$ZnNi_2O_4$	32.0-32.5	2.9-3.0

4. Conclusion

In concluding remarks, the sensitivity of nickel-doped zinc ferrite nanostructures were measured and optimized as a function of the doping level of nickel in the lattice structure of the zinc ferrite. The lattice parameters of the spinel structure are also likely to change due to the smaller ionic radius of Ni^{2+} compared to Fe^{3+}. This substitution can lead to a contraction of the unit cell. The $ZnNiFeO_4$ sensor achieved the lowest limit of detection (1.8 µM), while the $ZnFe_2O_4$ sensor had the highest limit of detection (8.0 µM) among the sensors tested.

Reference

[1] N. Ponpandian, P. balaya, and A. Narayanasamy, J. Phys. Cond. Matter, 14 (2002) 3221.

[2] A.A. Ahmed, N.A. Dahham, and G.G. Ali, Iraqi J. Appl. Phys., 20(3A) (2024) 505-510.

[3] M. Madagalam, M. Bartoli, M. Rosito, N. Bkangetti, M. Etzi Coller Pascuzzi, E. Padovano, B. Bonnelli, S. Carrar, and A. Tagliaferro, Small Struct., 4(12) (2023) 2300163.

[4] A.G. Cullis, L.T. Canham, P.D.J. Calcott, J. Appl. Phys., 82 (1997) 909-965.

[5] A.C.F.M. Costa, E. Tortella, M.R. Morelli, M. Kaufman, and R.H.G.A. Kiminami, J. Mater. Sci., 37(17) (2002) 3569-3572.

[6] A.K. Al-Kadumi and M. Al-Baghdadi, Iraqi J. Appl. Phys., 20(3B) (2024) 668-670.

[7] R. Liu, M. Lv, Q. Wang, H. Li, P. Guo, and X.S. Zhao, J. Magnet. Magnet. Mater., 424 (2017) 155-160.

[8] H. Yamaguchi and S. Murakami, Nucl. Fusion, 58(1) (2018) 016029.

[9] I.N. Yousif, A.T. Abdulhameed, A.M. Essmat, and A.I. Ahmed, Iraqi J. Appl. Phys., 20(3A) (2024) 565-568.

[10] J. Wang, Y. Xu, W. Li, Y. Yang, and F. Wang, J. Electrostat., 67(5) (2009) 815-826.

[11] J.N. Jasbijn, T.J. Tibsibim, and G.U. Jasbijn, Iraqi J. Appl. Phys., 18(1) (2022) 27-30

[12] M.A. Herrero, J. Guerra, V.S. Myers, M.V. Gomez, R.M. Crooks, and M. Prato, ACS Nano, 4 (2010) 905-912.

[13] N. Guettler, P. Knee, Q. Ye, and O. Tiedje, J. Coat. Technol. Res., 17(5) (2020) 1091-1104.

[14] U.A. Merhan and T.B. Simanja, Iraqi J. Appl. Phys., 18(1) (2022) 31-34

[15] X. Zhu, T. Liu, H. Zhao, L. Shi, X. Li, and M. Lan, Biosens. Bioelectron., 79 (2016) 449-456.

[16] Z. Qu, C. Mao, X. Zhu, J. Zhang, H. Jiang, and R. Chen, Ind. Eng. Chem. Res., 61(36) (2022) 13416-13430.

[17] A.A. Abbas, S.J. Hasan, I.M. Abdulmajeed, and S.Q. Hazaa, Iraqi J. Appl. Phys., 20(1) (2024) 91-95.

[18] A.Yu. Panarin, S.N. Terekhov, K.I. Kholostov, V.P. Bondarenko, Appl. Surf. Sci. 256 (2010) 6969-6976.

[19] F.B. Mohammed Ameen, G.G. Ali, and M.H. Younus, Iraqi J. Appl. Phys., 20(2B) (2024) 321-332.

[20] H. Yanada, S. Takag, and S. Mamiya, J. Electrostat., 74 (2015) 1-7.

[21] I.N. Yousif, M.J. Ali, and I.T. Tlayea, Iraqi J. Appl. Phys., 20(3A) (2024) 557-560.

[22] J. Zhang, Y. Liu, C. Mao, Z. Tang, H. Jiang, W. Xing, and R. Chen, Chem. Eng. Sci., 298 (2024) 120406.

[23] M. Feidt and D. Paulmier, Vacuum, 22(5) (1972) 181-182.

[24] M. Yamada, S. Seiler, H.W. Hendel, and H. Ikezi, Phys. Fluids, 20(3) (1977) 450-458.

[25] T. Zhang, S.A. Liao, L.X. Dai, J.W. Yu, W. Zhu, and Y.W. Zhang, Sci. China Mater., 61 (2018) 926-938.

[26] S.O. Kasap, A. Bhattacharyya and Z. Liang, Japanese J. Appl. Phys., 31(1R) (1992) 72-80.

[27] T. Adachi and T. Kawakubo, Phys. Rev. Special Topics Acceler. Beams, 16(5) (2013) 053501.

[28] X. Cui, L. Zheng, Q. Li, and Y. Guo, Ind. Eng. Chem. Res., 62(37) (2023) 14973-14985.

[29] Z. Cai and S. Park, Sens. Actuat. B: Chem., 367 (2022) 132090.

